

1 **Iodine speciation and size distribution in ambient aerosols at a coastal new particle formation hotspot of**
2 **China**

3 Huan Yu^{1,2}, Lili Ren², Xiangpeng Huang², Mingjie Xie², Jun He³, Hang Xiao⁴

4
5 1. Department of Atmospheric Science, School of Environmental Studies, China University of Geosciences,
6 Wuhan 430074, China

7 2. School of Environmental Science and Engineering, Nanjing University of Information Science and Technology,
8 Nanjing 210044, China

9 3. Department of Chemical and Environmental Engineering, University of Nottingham Ningbo China, Ningbo
10 315100, China

11 4. Ningbo Urban Environment Observation and Research Station, Institute of Urban Environment, Chinese
12 Academy of Sciences, Xiamen 361021, China

13 *Correspondence to:* Huan Yu (yuhuan_1981@163.com)

14 **Abstract**

15 Intense new particle formation (NPF) events were observed in the coastal atmosphere during algae growth and
16 farming season at Xiangshan Gulf of east China coast. High nucleation-mode iodine concentrations measured by
17 ultra-performance liquid chromatography coupled with quadrupole time-of-flight mass spectrometry
18 (UPLC/Q-TOF-MS) confirmed that the NPF events were induced by iodine species. Our study provided important
19 information of iodine speciation, size distribution and its role in NPF in the context of heavy air pollution in
20 China's coastal areas. For the first time, we identified 5 inorganic iodine species, 45 organic iodine compounds (35
21 molecular formulas) and a group of iodide-organic adducts in aerosols. The concentrations and size distributions of

22 iodine species down to 10 nanometers were measured during the iodine-induced NPF, continental NPF and
23 non-NPF days at the coastal site and compared to those at an inland site. The iodine in the above four types of
24 aerosol samples were characterized by iodate, aromatic iodine compounds, iodoacetic acid/iodopropenoic acid and
25 iodide-organic adducts, respectively. Iodide and organic iodine compounds were found in the nucleation mode
26 particles, however, it is still not clear whether they contributed to nucleation or just new particle growth. Wild algae,
27 as well as farmed algae, could be an important NPF source in China's coastal areas.

28 **1. Introduction**

29 Iodine is an essential trace element for all mammals (including human beings) and some aquatic plants. The
30 atmospheric impact of iodine includes ozone (O_3) depletion, altering HO_x and NO_x chemistry, mercury oxidation
31 and aerosol formation (Baker et al., 2001; O'Dowd et al., 2002). Marine emission sources of iodine containing
32 species in the atmosphere, such as iodomethane, molecular iodine (I_2), hypiodous acid (HOI) include marine biota
33 emission (Baker et al., 2000), sea surface iodide (I) activation by O_3 (Dixneuf et al., 2009; Mcfiggans et al., 2004;
34 Palmer et al., 2005; Sellegri et al., 2006) and sea surface bubble bursting (Seto and Duce, 1972). Continental iodine
35 sources include soil emission, fossil fuel and biomass combustions and industrial emissions (Redeker et al., 2000;
36 Sive et al., 2007). In recent years, much attention has been paid to the new particle formation (NPF) induced by
37 iodine species (Dall'Osto et al., 2018; Allan et al., 2015; Roscoe et al., 2015; Mahajan et al., 2011; McFiggans et al.,
38 2010; O'Dowd and De Leeuw, 2007; Grose et al., 2007; Yoon et al., 2006; O'Dowd et al., 2002). Based upon
39 current knowledge, a simplified scheme of iodine oxidation and nucleation is described as follows: volatile
40 iodocarbons or I_2 photolyse to I atoms, which react with O_3 to produce IO and IO_2 radicals; subsequently the
41 self-combination of IO and IO_2 forms iodine oxides I_2O_{2-5} ; iodine oxoacids $HIO_x(x=1-3)$ were produced either from
42 I_2O_{2-5} hydration or via the reaction of IO and IO_2 reaction with HO_x (Burkholder et al., 2004; Mart ín et al., 2013;

43 Sipil äet al., 2016); eventually, the clustering of $I_2O_{2.5}$ (or HIO_x) and the subsequent growth of these iodine particles
44 in the presence of other condensable vapors contribute to cloud condensation nuclei (CCN) so as to influence the
45 climate.

46 In the past, iodine concentration or speciation has been measured in natural and drinking water (Chen et al.,
47 2007; Liu et al., 2015; Wang and Jiang, 2008; Wei et al., 2007), precipitation (Gilfedder et al., 2007a; Yoshida et al.,
48 2007), soil (Yoshida et al., 2007), animal and macroalgae tissues (Hughes et al., 2006; Kaña et al., 2015; Shah et al.,
49 2005), edible salts (Yun et al., 2017; Zhang et al., 2010), and milk (Wang and Jiang, 2008). Previous measurements
50 in ambient aerosols showed only three iodine species: I^- , iodate (IO_3^-) and total soluble organic iodine (SOI) and
51 their relative concentration and size distribution varied largely with locations (e.g. inland, coastal or open ocean)
52 (Baker et al., 2001; Gilfedder et al., 2007a, b; Lai et al., 2008; Wimschneider and Heumann, 1995; Xu et al., 2010).
53 The majority of atmospheric models assume that IO_3^- would be the only stable and predominant iodine species in
54 aerosols (Saiz-Lopez et al., 2012), because I^- may be eventually oxidized to IO_3^- in aerosols or participate in
55 halogen activation to yield gaseous IX ($X=Cl, Br, I$). SOI deems to be formed from the reaction of aerosol organic
56 matter with HOI (Baker, 2005b). Organic iodine compounds are more toxic than I^- and IO_3^- to humans (Ding and
57 Zhang, 2009) and may play a key role in regulating the recycling of halogens to the gas phase. At present the
58 speciation of organic iodine compounds is the most significant knowledge gap in aerosol iodine chemistry
59 (Saiz-Lopez et al., 2012). Hence, to study the iodine speciation and size distribution will surely help to understand
60 their sources, transformation mechanisms and deposition rates in the atmosphere.

61 It still poses a challenge to determine organic iodine compounds in ambient aerosol. Up to date, there is no
62 detailed aerosol organic iodine speciation study in the literature. Total SOI was generally calculated as total soluble
63 iodine minus inorganic I^- and IO_3^- (Lai et al., 2008), which can be separated and quantified using an ion
64 chromatography coupled with inductively coupled plasma mass spectrometry (IC-ICP-MS). Although the peaks in

65 IC other than Γ and IO_3^- were suspected to be organic iodine (Gilfedder et al., 2007a, b, 2008), ICP-MS did not
66 provide molecular weight information. Without foreknown information of ion mass, molecular structure or
67 retention time (RT), neither liquid chromatography-MS (LC-MS) nor gas chromatography MS (GC- MS) can be
68 applied to identify and quantify unknown organic iodine in the aerosols. Unlike those in disinfection by-products or
69 iodine-rich seaweed, an individual organic iodine compound in a complex aerosol matrix is of extremely low
70 concentration. Based on our experience, organic iodine ions co-elute with many other interfering ions even after
71 chromatographic separation. As a result, it is difficult to apply even high resolution mass spectrometry to identify
72 unknown organic iodine compounds in the aerosols using MS and MS/MS techniques.

73 The populated coastal regions of eastern China are influenced by both industrial and marine emissions.
74 Growing algae population due to serious eutrophication in the coastal waters may promote iodine emission, which
75 make the coastal region a potential hotspot of new particle formation. Up to now, there has been no report of iodine
76 induced NPF in the places other than coastal sites of western Europe (e.g., Mace Head, Ireland; Roscoff, France; O
77 Grove, Spain), Tasmania (Cape Grim) and Polar regions. Besides, the iodine speciation measurement in particles
78 smaller than 100 nm is also scarce (Baker, 2005a; Baker, 2004; Gilfedder et al., 2008; Lai et al., 2008;
79 Wimschneider and Heumann, 1995). The purpose of our study is to characterize iodine speciation using the
80 ultra-performance liquid chromatography coupled with quadrupole time-of-flight mass spectrometry
81 (UPLC/Q-TOF-MS) and measure their concentrations in size segregated particles down to 10 nm diameter
82 collected during the NPF events observed at a coastal site of China. The comparison of iodine species between the
83 coastal site and an inland site will also be discussed.

84 2. Experiments

85 2.1 Sampling

86 A five-month campaign from January to May 2018 was carried out at Xiangshan Gulf of Zhejiang Province on
87 the east coast of China. The coastal observation site (29 °29'N, 121 °46'E, see Figure 1) is a small building about
88 40 m and 200 m away from the coastline at high tide and low tide, respectively. The Xiangshan Gulf is developed
89 as the largest algae cultivation area of Zhejiang Province. This feature makes the Xiangshan Gulf a potential
90 hotspot of iodine emission from wild or farmed algae. We used a scanning mobility particle spectrometer (SMPS)
91 and a Neutral Air Ion Spectrometer (NAIS) to monitor NPF events at the site. The statistical characteristics of new
92 particle formation at the observation site are not the focus of this paper. Instead, a nano Micro-Orifice Uniform
93 Deposit Impactor (nano-MOUDI, MSP Corp, Shoreview, MN) or a median-volume aerosol sampler were used to
94 collect size segregated 10 nm -18 μm aerosols or PM_{2.5} during typical NPF days. The 13-stage nano-MOUDI
95 provides d₅₀ cut-off sizes of 18, 10, 5.6, 3.2, 1.8, 1.0, 0.56, 0.32, 0.18, 0.10, 0.056, 0.032, 0.018 and 0.010 μm in
96 aerodynamic diameters when operating at a flow rate of 30 L min⁻¹. Offline method by high resolution mass
97 spectrometer was developed to analyze iodine in the aerosol samples.

98 Particle size distribution from 2 nm to 740 nm was obtained by integrating a long SMPS (TSI DMA3081 and
99 CPC3775; scanning range: 40-750 nm) and NAIS (scanning range:2-42nm) data. The SMPS sampled ambient air
100 from a 129 cm long and 1.0 cm inner diameter (I.D.) SS tube horizontally oriented with an airflow of 14 standard
101 L min⁻¹. NAIS sampling inlet was a 150 cm long and 32 cm inner diameter copper tube. The transport loss of
102 particles in the SMPS and NAIS inlets was corrected using size-dependent survival ratios. Scanning cycles of the
103 SMPS and NAIS were synchronized to 4 minutes. The NAIS measured positive ion, negative ion and total particles
104 alternately. The classification of iodine-induced NPF (hereafter, I-NPF event) and continental NPF events was

105 based on the size distribution observation and described in Section 3.1.

106 A nano-MOUDI sampling scheme was implemented according to the NPF classification. That is, one set of
107 nano-MOUDI samples was collected during the continental NPF days from February 11 to 13; one set of
108 nano-MOUDI samples was collected during the non-NPF days from April 16 to 18; one set of nano-MOUDI
109 samples was collected during the I-NPF days from May 9 to 11 and three sets of daily PM_{2.5} samples were collected
110 during the I-NPF days from April 25 to 27. Each set of nano-MOUDI samples was collected continuously for 72
111 hours, during which I-NPF or continental NPF occurred on a daily basis, so aerosol chemical composition features
112 of these two types of NPF events can be observed from offline analysis. In addition, as a comparison to the coastal
113 site, four sets of PM_{2.5} samples were randomly collected on January 14, April 15, April 25 and May 5 at an inland
114 urban site 200 km from the coast (see Figure 1). The description of the inland site can be found in Yu et al. (2016).
115 No simultaneous measurement of particle size distribution was made at the inland site.

116 The detailed sampling procedures for PM_{2.5} and nano-MOUDI are as follows. PM_{2.5} aerosols were collected
117 on 90 mm quartz fiber filters using a median-volume aerosol sampler (TH-150C, Wuhan Tianhong Ltd., China) at a
118 flow rate of 100 L min⁻¹ for 23 h. Since quartz fiber filters may absorb volatile iodine species like hydrogen iodide
119 (HI), which brings positive artifact to I⁻ measurement in aerosols, field blank filters were collected by placing a
120 HEPA filter in the upper stream of a quartz fiber filter. Two nano-MOUDIs were placed side by side to collect
121 10-100 nm (stages 10-13) and 100 nm-18 μm (stages 1-9) aerosols, respectively. Considering low aerosol mass
122 loading on stages 10-13, the chemical analysis of aerosols collected on 10-13 stages may be sensitive to the particle
123 bounce-off from upper stages 1-9, Therefore, aluminum foil filters on the stages 1-9 of the first nano-MOUDI were
124 silicon-greased to reduce potential bounce-off artifact on the filters of stages 10-13 that were sent for chemical
125 analysis. For the second nano-MOUDI, all filters were not silicon-greased but only the filters of stages 1-9 were
126 sent for chemical analysis. One set of field blank nano-MOUDI samples were also collected by drawing the air

127 through the nano-MOUDI with a HEPA filter attached to the inlet. Before sampling, the filters were baked in a
128 laboratory oven at ca. 500°C for 24 h to remove organics. After sampling, the filters were packed and stored in a
129 refrigerator below -20°C.

130 2.2 Chemical analysis

131 A quarter or half of a filter was put in a 10 mL amber vial with 1:1 v/v mixture of water (LCMS grade,
132 Aladdin, China) and methanol (LCMS grade, Adamas, China). The filter fraction was sonicated for 40 min and the
133 extract was filtered by a 0.2 µm PTFE membrane syringe filter. The eluate was evaporated to almost dryness in a
134 rotary evaporator below 40°C and subsequently re-dissolved in 0.5 mL water. After being centrifuged (12000 rpm)
135 for 30 min, the supernatant was collected for MS analysis using a Waters UPLC (BEH column, 1.7 µm column,
136 2.1×50mm) coupled with a Xevo G2 Q-TOF MS. A gradient eluent at flow rate 4mL/min was applied as below:
137 2/98 methanol/water for 0.5 min, linearly increased to 98/2 over 9.5 min, 98/2 held for 2 min, and returned to 2/98
138 for 3 min. The MS was operated in either positive or negative mode with a TOF resolving power of 32000 FWHM
139 (ESI+) or 28000 FWHM (ESI-). The MS was externally calibrated daily in the mass range 50–1200 using a 0.5
140 mM sodium formate solution. A real time Lockmass correction was applied by acquiring leucine-enkephalin
141 spectrum from a lock spray source. Optimized source parameters were as follows: capillary voltage -2.5 kV for
142 ESI- (or +3.0 kV for ESI+), desolvation gas flow 600 L h⁻¹ with temperature 450 °C and source temperature 120 °C.
143 Depending on the purpose, the QTOF was operated in 3 modes: low energy MS scan mode (in which molecular
144 ions are subject to in-source fragmentation only), high energy MS scan mode (in which molecular ions are subject
145 to both in-source fragmentation and collision induced dissociation) and MSMS mode (in which selected precursor
146 ions are subject to fragmentation with collision induced dissociation before entering TOF). Collision cell voltage
147 was scanned from 10 to 40 eV. Mass spectrum was acquired as continuum format and analyzed by the MassLynx

148 4.1 software. The procedure of identification and semi-quantification of iodine species will be explained in detail in
149 Section 3. To validate the semi-quantification by our procedure, 20 samples with relatively high iodine
150 concentration were also analyzed for total soluble iodine using Agilent 7500a ICP-MS (Agilent Technologies,
151 Santa Clara, CA, USA). To do that, 200 μl aerosol extract was diluted to 5 ml for injection and the iodine detection
152 limit of the ICP-MS was $0.1 \mu\text{g L}^{-1}$.

153 **3. Result and discussion**

154 Section 3.1 first discusses particle number size distribution patterns of two types of NPF events at the coastal
155 site. Section 3.2 discusses the identification and semi-quantification of iodine species in the ambient aerosols. The
156 speciation and size distribution of iodine species during the two types of NPF events at the coastal site are shown in
157 Section 3.3. The comparison of iodine species between the coastal site and the inland site is discussed in Section
158 3.4.

159 **3.1 Particle number size distribution patterns of iodine-induced NPF and continental NPF events**

160 Based on the particle size distribution data, we identified two types of NPF events. The first type of NPF
161 events was observed on 7 out of 54 non-raining observation days during the cold season from January to March.
162 Figure 2a shows the typical particle number size distributions of this type of NPF events from February 11 to 13.
163 As we can see in Figure 2a, the production of 2-7 nm neutral particles began at 8:00~9:00 and ceased at around
164 15:00. New particle formation appeared to be not associated with the low tide, but followed a nearly identical
165 variation with both solar radiation and daytime tide height. After the formation, new particles grew to about
166 100~200 nm in the middle of the night, following a typical banana-shape contour (Figure 2a, 1st row). These
167 features, together with the air mass backward trajectories originating from northwest inland of China (Figure S2),

168 confirm that this was a regional-scale continental NPF event. Air mass backward trajectories were computed using
169 the HYSPLIT (Hybrid Single-Particle Lagrangian Trajectory, NOAA/ARL) model (Draxler and Rolph 2003). N_{2-20} ,
170 number concentration of 2-20 nm particles, reached up to 7×10^4 - 1.3×10^5 cm^{-3} during this type of NPF events,
171 which is higher than the average N_{3-20} 2.5×10^4 cm^{-3} during the continental NPF events recorded by us at Nanjing,
172 the inland urban site in 2016 (Dai et al., 2017).

173 Strong NPF events were observed on 24 out of 33 non-raining observation days in April and May, which is the
174 growth and farming season of seaweed. That is, the second type of NPF events occurred almost every day from
175 April to May unless it was cloudy or rainy. As would be discussed in Section 3.3, high nucleation-mode iodine
176 concentration suggests these NPF events were induced by iodine. Figure 2b shows the typical particle number size
177 distributions from May 8 to 10. As can be seen, the production of 2-7 nm began at 9:00~10:00 and lasted until
178 18:00. There is a clear time lag of ~4 hours between solar radiation increase and the production of 2-7 nm. High
179 N_{2-7} (number concentration of 2-7 nm particles) seemed to be associated with low tide during 13:00-15:00. N_{2-20}
180 reached up to 7×10^6 cm^{-3} - 1×10^7 cm^{-3} , which is two orders of magnitude higher than those during the continental
181 NPF. The peak N_{2-20} values at this coastal site are also one order of magnitude higher than those recorded during the
182 most intense I-NPF events at Mace Head, Ireland (5×10^5 - 1×10^6 cm^{-3}) (O'Dowd et al., 2002). A clear nucleation
183 mode below 30 nm was seen on each sampling day and particles rarely grew beyond 30 nm at the coastal site of our
184 study. The “interrupted” growth pattern suggested that the NPF was limited in a relatively small area around the site.
185 Wild and farmed algae at the Xiangshan Gulf were likely the source of these high concentration nucleation mode
186 particles. In particular, during the harvesting season, the wet algae have to be dehydrated by exposing them to
187 sunlight for a few days before further processing or transportation. During this process, a large amount of iodine
188 vapors can be emitted and oxidized to produce new particles.

189 It has been reported from both field and laboratory studies that I-NPF is initiated by a pure negative ion

190 nucleation of HIO_3 (Sipilä et al., 2016). We examined neutral, positive and negative nanoparticle concentrations
191 measured by NAIS during the two types of events. It has been found that during the I-NPF events the negative ion
192 concentrations were $100 \pm 102\%$, $8 \pm 13\%$ and $58 \pm 32\%$ higher than those of positive ions in the size ranges of 0.8-2
193 nm, 2-7 nm and 7-20 nm, respectively. On the other hand, negative and positive ion concentrations in all
194 above-mentioned size ranges were almost the same during the continental NPF events (Figure 2a, row 4-6). The
195 neutral particle concentrations during I-NPF events were higher than those in continental NPF events by two orders
196 of magnitude; however, the ion concentrations were similar in both types of NPF events, which were in the
197 concentration range of 100-1000 cm^{-3} in all size bins. As a result, the ion/neutral particle ratios were on the order of
198 10^{-5} (2-7 nm) and 10^{-4} (7-20 nm) during the I-NPF events and 10^{-3} (2-7 nm) and 10^{-2} (7-20 nm) during the
199 continental NPF events, indicating the contribution of ions to total particles was negligible at least in > 2 nm size
200 range in both types of NPF events.

201 **3.2 Iodine speciation and semi-quantification**

202 The high resolution LC-MS offers the prospect of identifying unknown organic compounds in complex
203 samples. Previous studies identified unknown organic iodine compounds in disinfected drinking water and seaweed
204 base on a strategy that the retention time and accurate mass of iodine-containing precursor ions can be selectively
205 determined by searching their product ion I^- (m/z 126.9) in MS/MS experiments (Ding et al., 2009; Yang et al.,
206 2016). Unfortunately, their strategy does not work for our aerosol samples because of two difficulties. First, we
207 found that most of iodine-containing ions in our samples were dissociated to release I^- due to in-source
208 fragmentation even in the most gentle ionization condition (e.g., low capillary voltage, low source temperature and
209 desolvation temperature). This can be seen from Figure 3a that extracted ion chromatograms of m/z 126.9039 are
210 of similar intensity in low energy MS scan mode (in-source fragmentation only) and high energy MS scan mode

211 (in-source fragmentation plus collision induced dissociation). In this situation, it is impossible to select
212 unfragmented iodine-containing precursor ions for MSMS experiments. Second, even if organic iodine compounds
213 can survive from in-source fragmentation, there are many co-eluting background interfering ions. It is time and
214 labor consuming to search I^- from all co-eluting molecular ions using MSMS experiments. This often becomes
215 impractical because small organic iodine ions and other neighboring ions often appear in the same precursor
216 isolation window of quadrupole.

217 *Iodide-organic adducts*

218 For reversed phase HPLC, ionic compounds elute earliest followed by non-ionic organics with longer
219 retention time. In our case, ionic I^- , IO_x^- and other strong Lewis acids elute with $RT < 1$ min, as can be seen from the
220 extracted m/z 126.9039 chromatogram of pure potassium iodide solution (1 mmol L^{-1}) in Figure 3b. The I^- peaks
221 that eluted at $RT > 1$ min in low energy MS scan mode (Figure 3a), on the other hand, can only be resulted from the
222 dissociation of weakly bound iodine-containing organic precursors via in-source fragmentation. I^- is an
223 electronegative weak base, which can bind with hydroxyl, acid or keto- groups to form adducts depending upon the
224 polarity and H-bonding capability of organic compounds (Lee et al., 2014). These iodine-containing organics that
225 dissociated to release I^- in the ESI source are thus attributed to iodide-organic adducts in our study and the total
226 peak area of extracted ion chromatogram of m/z 126.9039 after RT 1 min is assumed to be proportional to their
227 total concentration. Our experiment presented in Figure 3b-3d partly supported the above hypothesis. No I^- peak
228 was detected after RT 1 min in the extracted m/z 126.9039 chromatograms of pure KI solution (1 mmol L^{-1} , Figure
229 3b) or an aerosol extract with low concentration of iodine (Figure 3c). However, when the aerosol extract was
230 mixed with KI solution for another analysis, elevated I^- peaks in low energy MS scan mode (blue line, Figure 3d)
231 indicated the formation of iodide-organic adducts. Furthermore, when collision induced dissociation was applied,

232 no additional I peaks showed up in high energy MS scan mode (red line, Figure 3d). Such an observation implies
233 that (1) iodide-organic adducts were formed in the aerosol extract+KI mixture but were easily dissociated in the
234 low energy MS scan mode and (2) no stable organic iodine compounds were formed in the aerosol extract+KI
235 mixture. This is also confirmed by the fact that no new ions were formed by comparing the mass spectra of aerosol
236 extract before and after KI addition.

237 *Organic iodine compounds*

238 On the other hand, the identities of those stable organic iodine compounds, i.e., the compounds with C-I bond
239 that are not or partially dissociated in the ESI source, are still unknown but their atmospheric chemistry may be of
240 more interest. To bypass the difficulty as discussed above, a signal amplification approach has been applied in this
241 study to identify these unknown organic iodine compounds, for which the detailed steps are shown in Figure 4. The
242 approach is analogous to searching a secondary organic aerosol (SOA) tracer in ambient aerosols after its identity
243 as VOC oxidation product is confirmed by smog chamber simulation. A portion of low iodine aerosol extract+KI
244 mixture was added with H₂O₂ solution (10 mmol L⁻¹). After reaction for 4 h, the mixture was injected for low and
245 high energy MS scans. As compared to the chromatograms of the untreated mixture (Figure 3d), a considerable
246 amount of stable organic iodine compounds were formed but dissociated only in high energy MS scan (red curve in
247 Figure 3e), in addition to the formation of more iodide-organic adducts (low energy MS scan, blue curve in Figure
248 3e). These organic iodine compounds are believed to be from the reactions between aerosol organics and HOI that
249 is produced via H₂O₂+I reaction.

250 The identities of these organic iodine compounds can be obtained by comparing MS scan mass spectra (low
251 energy) before and after the H₂O₂ addition using mass defect (MD) vs. m/z diagram. The mass spectrum was
252 reconstructed by integrating over RT 0-15 min. All ions above background intensity of 10⁴ are shown in Figure 5 as

253 dots and circles to stand for the samples before and after H₂O₂ addition, respectively. Benefiting from the large
254 negative mass defect of iodine (-0.0961), the mass defects of newly-formed organic iodine compound should be in
255 the range of -0.3~0, which makes them to be distinguished easily from non-iodine containing ions. Therefore, each
256 red circle without a black dot in -0.3~0 mass defect range in Figure 5 should stand for an organic iodine compound
257 that was newly formed after the addition of H₂O₂ into aerosol extract+KI mixture. These potential organic iodine
258 ions were further selected for MSMS experiments to confirm that their fragments contained I. Since mass
259 assignment is more accurate for an amplified symmetrical peak than a small shoulder peak, the amplification of
260 organic iodine compound concentrations helps to obtain accurate masses of potential iodine organic compounds in
261 ambient aerosols. After that, their retention time information in the UPLC was acquired by extracting their ion
262 chromatograms from low energy MS scan data. Following the same procedure, two PM_{2.5} samples collected at the
263 inland site and two PM_{2.5} samples collected at the coastal site were treated using KI and H₂O₂ (or O₃ solution) and
264 analyzed using MD vs. m/z diagrams in both ESI+ and ESI- modes (Step 1, Figure 4).

265 In step 2, the elemental compositions of organic iodine compounds were calculated from the accurate masses
266 within 1 mDa mass tolerance allowing the elements C, H, N, O, S and I and confirmed by their isotope patterns.
267 The correctness of calculated molecular formulas was further restricted by the matching of at least one sound
268 structure in ChemSpider database. Consequently, a total of 80 formulas (57 in negative mode and 23 in positive
269 mode) were obtained, each of which should represent an organic iodine compound and its isomers. Because both
270 H₂O₂ and O₃ are important oxidants in atmospheric aerosols, the organic iodine compounds formed in Step 1 may
271 also exist in real aerosol samples via the same reaction mechanism in the atmosphere. Therefore, in Step 3 these
272 newly identified 80 formulas were searched in real aerosol samples using a targeted screening strategy based on
273 their accurate mass and retention time. At last, 35 organic iodine formulas were detected, at least once, in our
274 aerosol samples including the PM_{2.5} samples and the size-segregated aerosol samples from all nano-MOUDI stages

275 (Table 1). The other formulas were not detected in any of the aerosol samples, probably due to their slower
276 production rate or the absence of corresponding organic precursors in the atmosphere. The number of isomers listed
277 in the second column of Table 1 is based on the number of ion chromatographic peaks observed for given m/z
278 values in the real aerosol samples. The total 45 isomer peaks, as well as their retention times, are shown in Figure
279 S1. Hence, there are in total 45 organic iodine compounds detected in our samples.

280 As shown in Table 1, 35 molecular formulas were classified into four groups: 5 non-aromatic formulas and 30
281 aromatic formulas including 16 CHOI formulas, 3 CHNI formulas and 11 CHONI formulas. The 5 non-aromatic
282 formulas are assigned to iodoacetic acid, diiodoacetic acid, iodopropenoic acid, iodomethanesulfonic acid and
283 diiodomethane. The first 4 compounds are electrophilic substitution products of alpha-H of organic acids by I^+ from
284 HOI or I_2 . Diiodomethane is probably from gas-particle partitioning or the product of iodoform reaction of methyl
285 ketones. Iodoacetic acid was identified in 9 of 10 samples collected from the coastal and inland sites. The other 4
286 non-aromatic compounds, however, were mostly found at the coastal site.

287 30 CHOI, CHONI and CHNI formulas are assigned to aromatic compounds that are prone to electrophilic
288 substitution by I^+ . The formulas observed in ESI- mode are expected to have a carboxyl or phenol group, while
289 those observed in ESI+ mode should be aromatic or heterocyclic amines. 16 CHOI formulas are iodinated phenols,
290 substituted benzoic acids or phenolic acids. The 3 most frequently detected formulas are $C_8H_7O_2I$, $C_7H_5O_4I$,
291 $C_7H_5O_2I$. CHONI formulas with 3-5 O atoms detected in ESI- mode are iodinated nitrophenol, nitronaphthol or
292 nitrobenzoic acid. CHONI formulas with 1 O atom detected in ESI+ mode are iodinated hydroxyaniline, pyridinol,
293 or quinolinol. The most frequently detected CHONI compounds are $C_6H_4NO_4I$, $C_{10}H_6NO_3I$ and $C_6H_4NO_3I$. CHNI
294 formulas are heterocyclic amines (i.e., pyrazoles, imidazoles and triazoles), among which $C_7H_{11}N_2I$ was detected in
295 4 out of 10 samples.

296 Further assignment of the exact identity for the above formulas is impractical, because these 35 molecular

297 formulas probably stand for hundreds of isomers, for most of which no commercial standards are available.
298 Nevertheless, the identities of 4 compounds have been confirmed including iodoacetic acid ($C_2H_3O_2I$),
299 3-iodo-2-propenoic acid ($C_3H_3O_2I$), 3-iodo-benzoic acid ($C_7H_5O_2I$) and 2-hydroxy-5-iodopyridine (C_5H_4NOI)
300 according to the retention times of their commercial standards. These 4 compounds are identifiable because they
301 have no or very few isomers, of which the commercial standards can be procured. Subsequently, these four
302 compounds can be used as surrogate standards to semi-quantify the concentrations of other organic iodine species.

303 *Inorganic iodine species*

304 In addition to the above organic iodine compounds, some inorganic iodine species were also detected. Figure 6
305 shows the integrated mass spectrum of molecular ions between RT 0.5-0.7 min obtained by low energy MS scan of
306 an S13 nano-MOUDI sample (10-18 nm particles) collected during the I-NPF days. The most abundant species is
307 IO_3^- , followed by I^- and HSO_4^- . I_3^- was also observed, probably due to the adduct formation between I^- and I_2 . IO_2^-
308 and IO^- are detectable, but their abundances are two orders of magnitude lower than IO_3^- . Iodine oxides $I_2O_{2.5}$ were
309 not ionizable by the ESI source, but they might have been hydrated to HIO_x and detected as IO_x^- (Sipil äet al. 2016).
310 Iodide-metal complexes like CuI_2^- , $Cu_2I_3^-$, ZnI_3^- and $CuI_2(HCN)(HCl)^-$ were observed in $PM_{2.5}$ samples but not in
311 size-segregated nano-MOUDI samples. Cu^+ and Zn^{2+} are typical coarse mode components. The observation thus
312 indicated that the iodide-metal complexes detected in the $PM_{2.5}$ samples were formed only after fine- and
313 coarse-mode components were mixed in the sample extract. To avoid artificial formation of iodide-metal
314 complexes during the sample extraction process, our result highlights the importance of collecting $PM_{0.5}$, PM_1 or
315 size-segregated samples instead of $PM_{2.5}$ or PM_{10} .

316 *Semi-quantification of identified iodine species*

317 So far 35 organic iodine formulas (45 isomer peaks) and 5 inorganic iodine anions have been identified. In

318 order to know their size distributions and relative abundances in different types of samples, the following strategy
319 was applied to semi-quantify these iodine species (step 4, Figure 4): external calibration curves of peak area vs.
320 concentration were established by analyzing standard solutions of KI, KIO₃, iodoacetic acid, 3-iodo-2-propenoic
321 acid, 3-iodo-benzoic acid and 2-hydroxy-5-iodopyridine. I⁻, I₃⁻ and iodide-organic adducts were quantified using KI
322 as a surrogate standard by assuming their ionization efficiencies are similar in ESI⁻ mode. The peak area of
323 iodide-organic adducts was calculated as the total peak area of extracted ion chromatogram of m/z 126.9039 after
324 RT 1 min. Iodide-metal complexes like CuI₂⁻, Cu₂I₃⁻, ZnI₃⁻ and CuI₂(HCN)(HCl)⁻, if present, were also quantified
325 using KI but counted as I⁻. IO₃⁻, IO₂⁻ and IO⁻ were quantified using KIO₃ by assuming iodate, iodite and hypiodite
326 have similar ionization efficiencies. Iodoacetic acid and 3-iodo-2-propenoic acid were quantified with their
327 respective standards. The other 3 non-aromatic compounds diiodoacetic acid, iodo-methanesulfonic acid and
328 diiodomethane were quantified using surrogate standard iodoacetic acid. All CHO and CHNO compounds observed
329 in ESI⁻ mode were quantified using 3-iodo-benzoic acid, because they have similar structure of a carboxyl or
330 phenol group attached to aromatic rings. All CHNO and CHN compounds observed in ESI⁺ mode were quantified
331 with 2-hydroxy-5-iodopyridine by assuming these aromatic or heterocyclic amines have similar ionization
332 efficiencies. Due to the low amounts of individual aromatic compounds, a total concentration of all aromatic iodine
333 compounds detected was presented for each sample. Field blank filters were processed in the same way as sample
334 filters. No signals above MS background were detected in the field blank filters for the iodine species other than I⁻
335 and IO₃⁻. The MS signals of I⁻ and IO₃⁻ in the field blanks were comparable to those in the sample filters without
336 iodine loading (e.g., the nano-MOUDI filters in the size bins larger than nucleation mode during the I-NPF days),
337 but less than 1.3% of those in the sample filters with iodine loading. The MS signals of I⁻ and IO₃⁻ in the field blank
338 were then subtracted from the aerosol samples.

339 There are a few limitations in the above-mentioned strategy. First, the use of surrogate standards can only be

340 regarded as semi-quantification for unassigned species. Second, it is still possible that some unknown organic
341 iodine compounds are missed by our method shown in Figure 4. Third, inorganic iodine ions that elute around
342 0.5-0.7 min are prone to a stronger matrix ion suppression effect than organic compounds. The underestimation
343 may be the most serious if there are high concentrations of co-eluting sulfate, nitrate and ammonium in the aerosol
344 samples of accumulation mode. After UPLC/Q-TOF-MS measurement, we selected 13 samples with relatively high
345 iodine concentrations for ICP-MS analysis, including 3 PM_{2.5} samples and 10 size-segregated samples from 10 nm
346 to 1.8 μm collected during the NPF days. A linear regression analysis was conducted between the sum of all iodine
347 species measured by this method and the total iodine measured by ICP-MS. As shown in Figure 7, the total iodine
348 concentration analyzed by our method is 90.5% on average of that obtained by ICP-MS with a R² of 0.94. In spite
349 of the above uncertainties, our method provided a lower-limit estimate of iodine concentrations in ambient aerosols.

350 **3.3 Concentration and size distribution of iodine species during the NPF days at the coastal site**

351 We compared the total concentrations (Figure 8) and mass size distributions (Figure 9) of iodine species in 10
352 nm-18 μm particles during the I-NPF, continental NPF and non-NPF days at the coastal site. The particle number
353 size distributions during the same NPF days have been shown in Figure 2. It should be noted that, identical to
354 previous aerosol iodine speciation studies, the concentration reported here (pmol m⁻³) is an average over the entire
355 period of 3 sampling days. Thus, iodine concentrations during the intense NPF periods should be higher than the
356 values reported in this work. Continuous mass size distribution was fitted from the measured size-segregated mass
357 concentration data by assuming multimodal lognormal size distributions (Yu et al. 2010). Size distribution of
358 sulfate (HSO₄⁻) was also shown (μg m⁻³) in Figure 9. Although not highly accurate, relative distribution in different
359 sizes is less affected by the uncertainties of semi-quantification.

360 The highest total iodine concentration 126.3 pmol m⁻³ was found during the I-NPF days, which was 3.1 and

361 5.5 times higher than those during the continental NPF and non-NPF events, respectively. As shown in Figure 9a,
362 all iodine species except iodoacetic acid were characterized by a nucleation mode with mode diameters between
363 22-35 nm during the I-NPF days. This clearly shows that iodine was the NPF precursor in this type of NPF events.
364 The most remarkable iodine species during the I-NPF days is IO_3^- with a mole fraction of 42.5%. This is consistent
365 with the recent observation that HIO_3 is the key nucleating precursor in I-NPF event (Sipilä et al., 2016). On the
366 other hand, the sum of iodide ($[\text{I}^-] + [\text{I}_3^-]$) and iodide-organic adducts accounted for ~50 % of total iodine in newly
367 formed iodine particles. The presence of high iodide concentration in clusters or new particles has not been
368 reported by previous field or laboratory measurements using CI-API-TOF or AMS (O'Dowd et al., 2002;
369 McFiggans et al., 2004; Sipilä et al., 2016). Iodide is most likely originating from the partitioning of gaseous
370 precursor HI formed during the photolysis of I_2 or iodomethane. HI itself is not a good nucleation precursor due to
371 the lack of H-bond or halogen bond, but our measurement suggests that HI might contribute to new particle growth
372 in the size range as small as 10-18 nm. The finding of HSO_4^- in nucleation mode (Figure 6 and 9a) indicates that
373 H_2SO_4 also contributed to new particle growth during the I-NPF days. This is consistent with previous laboratory
374 observations of efficient uptake of H_2SO_4 onto humidified iodine oxide particles below 20 nm (Saunders et al.
375 2010).

376 Although organic iodine compounds were most frequently found in the I-NPF samples (Table 1), they
377 accounted for only 6.8% of total iodine in the newly formed iodine particles. Considering the short lifetime of new
378 particles in the atmosphere, organic iodine compounds were most likely from the heterogeneous uptake of gaseous
379 HOI (formation route: $\text{I} \rightarrow \text{IO} \rightarrow \text{HOI}$) and subsequent reactions with organics in the new particles. One exception
380 is iodoacetic acid that was characterized by a smaller accumulation mode and a larger coarse mode. Backward
381 trajectory analysis showed that air masses moved from the open ocean of East China Sea during the I-NPF days
382 (Figure S2). The unique size distribution of iodoacetic acid indicates that direct sea salt emission was probably its

383 major source.

384 Lower iodine concentrations during the continental NPF days and non-NPF days might be due to relatively
385 low iodine emission rate or transformation rate (from gaseous emission to particles) in non-algae-growth season or
386 cloudy days. Iodine during the continental NPF days was characterized by an accumulation mode with mode
387 diameters between 500-700 nm (Figure 9b), except that iodoacetic acid had a coarse mode and 3-iodo-2-propenoic
388 acid had a 60 nm Aitken mode. The absence of nucleation mode for most of iodine compounds implies that iodine
389 was unlikely to be an important NPF precursor in the continental NPF. Despite different size distribution from
390 I-NPF, the mole fraction of iodide and iodide-organic adducts were again ~50% of total iodine during the
391 continental NPF. The outstanding species in the continental NPF days were aromatic iodine compounds that
392 accounted for 30% of total iodine. This is not surprising because air masses from inland areas of China on these
393 days might contain a large amount of anthropogenic aromatic substances. Upon arrival in the coastal region, the
394 uptake of gaseous HI, HOI or IONO₂ onto these anthropogenic particles and the subsequent aerosol phase reactions
395 between I, H₂O₂/O₃, HOI and aromatic compounds are hypothesized to be the formation mechanism of aromatic
396 iodine compounds.

397 Iodoacetic acid and 3-iodo-2-propenoic acid surprisingly accounted for 44.3% of total iodine concentration
398 (22.8 pmol m⁻³) during the non-NPF days. The high iodoacetic acid concentration, together with its presence in
399 coarse mode, again suggests its unique source associated with sea salt emission. 3-iodo-2-propenoic acid during
400 the non-NPF days and continental NPF days was characterized by a bimodal distribution with mode diameters
401 around 1 μm and 50-63 nm. In contrast, the bimodal distribution was replaced by a single small nucleation mode
402 during the I-NPF days. The sources of 3-iodo-2-propenoic acid and iodoacetic acid became more important during
403 the non-NPF days and merit more investigation.

404 3.4 Comparison between coastal site and inland site

405 Table 2 gives a comparative overview of iodine species in $PM_{2.5}$ between the inland urban site and the coastal
406 site. The coastal samples include the 3 sets of nano-MOUDI data presented in Figure 8, from which the
407 concentrations of various iodine species in 10 nm - 3.2 μm particles were extracted to approximate $PM_{2.5}$; the rest
408 of data were acquired by directly analyzing the $PM_{2.5}$ samples. It is found that total iodine was in the range of
409 6.5-11.2 and 19.5-122.6 pmol m^{-3} at the inland and coastal sites, respectively. Larger variation of iodine
410 concentrations at the coastal site is due to the inclusion of both I-NPF and non-NPF samples. The concentrations of
411 nearly all iodine species at the inland site were lower than those at the coastal site. This indicates that there were no
412 or relatively weak iodine emission sources surrounding the inland site. Our total iodine concentrations are in the
413 same order of magnitude as those reported at Mace Head (10-532 pmol m^{-3} , Gilfedder et al., 2008), an Ireland
414 coastal site where iodine NPF has long been reported, and Regensburg, an inland site of southern Germany
415 (15.7-61.3 pmol m^{-3} , Wimschneider and Heumann, 1995), although their maximum values are higher than ours.

416 A negligible amount of iodate (1.1%) was detected in only 1 out of the 4 inland samples. In fact, the
417 concentration of iodate was also low on the days without I-NPF events at the coastal site (on average $7 \pm 1\%$).
418 Therefore, iodate is a predominant species only in newly formed particles (Figure 9) and its concentration might be
419 reduced soon in the aging process via reactions like $\text{IO}_3^- + \text{I}^- + 6\text{H}^+ \rightarrow 3\text{I}_2 + 3\text{H}_2\text{O}$ (Pechtl et al., 2007). The mole
420 fractions of iodide were $23 \pm 9\%$ and $31 \pm 14\%$ at the inland and coastal sites, respectively. Following the old
421 definition, the iodine species other than I^- and IO_3^- were calculated as soluble organic iodine (SOI). Our finding is
422 that newly formed iodine particles were mostly composed of inorganic I^- and IO_3^- ($68 \pm 20\%$ of the total iodine), but
423 SOI fraction increased to account for on average $76 \pm 7\%$ of total iodine in the aged particles. Among the SOI
424 species, the largest fraction $64 \pm 8\%$ was attributed to iodide-organic adducts at the inland site, followed by
425 aromatic iodine ($12 \pm 3\%$) and iodoacetic acid ($1.6 \pm 1.0\%$). All other species were not detectable or of negligible

426 amounts.

427 Table 2 clearly shows that more information on the speciation of soluble organic iodine in the aerosol samples
428 is provided in this study as compared to previous studies. In particular, a portion of iodine technically defined as
429 iodide-organic adducts was reported in our study for the first time, because they cannot survive in electrospray
430 ionization processes even in the most gentle source conditions, due to the weak bounding strength of I⁻ with
431 organics. I-organic adducts accounted for 64 ± 8% in the inland urban samples and 31 ± 16% in the coastal samples.
432 Using IC-ICP-MS method, this portion of iodine is likely counted towards organic iodine compounds. Our analysis
433 shows that this portion of iodine adducts can be attributed to neither stable organic iodine compounds nor free I⁻ ion.
434 Under certain condition, e.g., pH value, iodide-organic adducts probably release free I⁻ ion in the ambient aerosols.

435 **4. Conclusion**

436 Intense new particle formation events were observed during the algae growth and farming season at
437 Xiangshan Gulf, a coastal algaculture area of China. The high iodine concentration in nucleation mode particles
438 measured by UPLC/Q-TOF-MS confirmed that the NPF events were induced by iodine species. This is the first
439 study to investigate iodine-induced NPF in a place other than the coastal locations of western Europe, Tasmania and
440 Polar regions. China produced 58% of global cultivated seaweed production (11 million tons in 2010, Nayar and
441 Bott, 2014). Iodine is likely emitted to the atmosphere and transformed to nano particles during the farming,
442 harvesting and processing of cultivated seaweed. Growing algae population due to serious eutrophication in the
443 coastal waters of China also promotes iodine emission. Therefore, wild algae, as well as farmed algae, could be an
444 important source of new particle formation in the coastal areas of China.

445 Using UPLC/Q-TOF-MS, inorganic I⁻, IO_x⁻ and I₃⁻ were easily identified according to their accurate ion mass.
446 A large portion of iodide was observed to exist as weakly bound iodide-organic adducts. A signal amplification

447 approach was applied to look for organic iodine compounds, i.e., the compounds with C-I bond. For the first time,
448 35 molecular formulas, or 45 organic compounds according to the number of isomer peaks, were identified in
449 ambient aerosols. Iodine species on the I-NPF days and continental NPF days were characterized by a nucleation
450 mode and an accumulation mode, respectively. For the first time, high concentration of Γ was observed in particles
451 as small as 10-18 nm, suggesting gaseous HI may contribute to new particle growth in the I-NPF events. Iodate was
452 a remarkable species in only newly formed particles and was reduced in the aging process. Newly formed iodine
453 particles were mostly composed of inorganic Γ and IO_3^- , but SOI ($[\text{total iodine}] - [\Gamma] - [\text{IO}_3^-]$) accounted for the
454 majority of iodine in the aged particles. Generally speaking, organic iodine compounds resided in the same particle
455 mode as inorganic iodide. It is still not clear whether organic iodine compounds contributed to nucleation or just the
456 growth of new particles via iodine reactions with organics. During the continental NPF days, the outstanding iodine
457 species is aromatic iodine compounds in the accumulation mode that accounted for 30% of total iodine. Those
458 aromatic iodine compounds were probably formed from aqueous phase reactions between Γ , $\text{H}_2\text{O}_2/\text{O}_3$, HOI and
459 aromatic organic compounds during in-cloud processing. The unexpected iodoacetic acid in the coarse mode that
460 direct sea salt emission was probably its major source.

461 Our study provided important information of iodine speciation, concentration and size distribution in the
462 context of heavy air pollution in China's coastal areas. However, source, gas-particle partitioning and the role of
463 these iodine species in NPF are largely speculative. Moreover, the chemical composition and the role of iodine in
464 cluster sizes (1-3 nm) are still unknown. Simultaneous measurement of gaseous iodine precursors like I_2 , HI, HIO_x
465 and IO_x using online instruments like CI-Api-TOF and DOAS are needed to elucidate the above questions. On the
466 other hand, more field measurements at multiple sites are required to test on what spatial scale iodine NPF might be
467 of relevance, in competition with other NPF precursors.

468

469 **Author contribution**

470 H.Y. and H.X. designed and organized the study. X.H. and L.R. conducted the field measurements. H.Y. and
471 L.R. performed the instrumental experiments and data analysis. H.Y. and R.L. wrote the paper. M.X. and J.H.
472 contributed to data interpretation and paper writing.

473

474 **Acknowledgements**

475 The authors would like to thank the National Key Research and Development Program of China
476 (2016YFC0203100), the National Science Foundation of China (grant numbers. 41675124) and Jiangsu Specially
477 Appointed Professor Grant.

478 **References**

- 479 Allan, J.D., Williams, P.I., Najera, J., Whitehead, J.D., Flynn, M.J., Taylor, J.W., Liu, D., Darbyshire, E., Carpenter,
480 L.J., Chance, R., Andrews, S.J., Hackenberg, S.C., McFiggans, G.: Iodine observed in new particle formation
481 events in the Arctic atmosphere during ACCACIA, *Atmos. Chem. Phys.*, 15, 5599-5609, doi:
482 10.5194/acp-15-5599-2015, 2015.
- 483 Baker, A.: Marine aerosol iodine chemistry: The importance of soluble organic iodine, *Environ. Chem.*, 2, 295-298,
484 doi: 10.1071/EN05070, 2005.
- 485 Baker, A.R.: Inorganic iodine speciation in tropical Atlantic aerosol, *Geophys. Res. Lett.*, 31, 187-206,
486 doi:10.1029/2004GL020144, 2004.
- 487 Baker, A.R., Sj, C.M.P., Jickells, T.D., Thompson, D.: Iodine concentration and availability in atmospheric aerosol,
488 *Atmos. Environ.*, 34, 4331-4336, doi: 10.1016/s1352-2310(00)00208-9, 2000.
- 489 Baker, A.R., Tunnicliffe, C., Jickells, T.D.: Iodine speciation and deposition fluxes from the marine atmosphere, J.

490 Geophys. Res-Atmos., 106, 28743-28749, doi: 10.1029/2000JD000004, 2001.

491 Burkholder, J., Curtius, J., Ravishankara, A., Lovejoy, E.: Laboratory studies of the homogeneous nucleation of
492 iodine oxides, *Atmos. Chem. Phys.*, 4, 19-34, doi: 1680-7324/acp/2004-4-19, 2004.

493 Chen, Z.L., Megharaj, M., Naidu, R.: Speciation of iodate and iodide in seawater by non-suppressed ion
494 chromatography with inductively coupled plasma mass spectrometry, *Talanta*, 72, 1842-1846, doi:10.
495 1016/j.talanta.2007.02.014, 2007.

496 Dai, L., Wang, H., Zhou, L., An, J., Tang, L., Lu, C., Yan, W., Liu, R., Kong, S., Chen, M.J.: Regional and local
497 new particle formation events observed in the Yangtze River Delta region, China: Simultaneous NPF
498 measurements at 2 sites, *J Geophys. Res-atmos.*, 122(4):2389-2402, doi: 10.1002 /2016JD026030, 2017.

499 Dall'Osto, M., Simo, R., Harrison, R. M., Beddows, D. C. S., Saiz-Lopez, A., Lange, R., Skov, H., Nøjgaard, J. K.,
500 Nielsen, I. E., and Massling, A.: Abiotic and biotic sources influencing spring new particle formation in North
501 East Greenland, *Atmos. Environ.*, 190, 126-34, doi:10.1016/j.atmosenv.2018.07.019, 2018.

502 Draxler R R, Rolph G D: HYSPLIT-hybrid single particle lagrangian integrated trajectory model 2003 (NOAA Air
503 Resources Laboratory: Silver Spring, MD) <http://ready.arl.noaa.gov/HYSPLIT.php>, 2003.

504 Ding, G., Zhang, X.: A picture of polar iodinated disinfection byproducts in drinking water by
505 (UPLC/ESI-tqMS), *Environ. Sci. Technol.*, 43, 9287, doi:10.1021/es901821a, 2009.

506 Dixneuf, S., Ruth, A.A., Vaughan, S., Varma, R.M., Orphal, J.: The time dependence of molecular iodine emission
507 from *Laminaria digitata*, *Atmos. Chem. Phys.*, 9, 823-829, doi:10.5194/ acp-9-823-2009, 2009.

508 Gilfedder, B. S., Lai, S. C., Petri, M., Biester, H., Hoffmann, T.: Iodine speciation in rain, snow and aerosols, *Atmos.*
509 *Chem. Phys.*, 8, 6069-6084, doi: 10.5194/acp-8-6069-2008, 2008.

510 Gilfedder, B.S., Petri, M., Biester, H.: Iodine Speciation in Rain and Snow, *Nucl. Atmos. Aero.*, doi:
511 10.1007/978-1-4020-6475-3_108, 2007a.

512 Gilfedder, B.S., Petri, M., Biester, H.: Iodine speciation in rain and snow: Implications for the atmospheric iodine
513 sink, *J. Geophys. Res-atmos.*, 112, doi:10.1029/2006JD007356, 2007b.

514 Grose, M.R., Caine, J.M., McMinn, A., Gibson, J.A.E.: Coastal marine methyl iodide source and links to new
515 particle formation at Cape Grim during February 2006. *Environ Chem* 4, 172-177. doi: 10.1071/EN07008,
516 2007

517 Hughes, C., Malin, G., Nightingale, P.D., Liss, P.S.: The Effect of Light Stress on the Release of Volatile
518 Iodocarbons by Three Species of Marine Microalgae, *Limnol. Oceanogr.*, 51, 2849-2854,
519 doi:10.4319/lo.2006.51.6.2849, 2006.

520 Kaňa, A., Hrubá, L., Vosmanská, M., Mestek, O.: Analysis of iodine and its species in animal tissues, *Chemical*.
521 *Spec. Bioavailab.*, 27, 81-91, doi: 10.1080/09542299.2015.1087160, 2015.

522 Lai, S.C., Hoffmann, T., Xie, Z.Q.: Iodine speciation in marine aerosols along a 30,000 km round - trip cruise path
523 from Shanghai, China to Prydz Bay, Antarctica, *Geophys. Res. Lett.*, 35, L21803, doi:10.1029/2008gl035492,
524 2008.

525 Lee, B. H., Lopez-Hilfiker, F. D., Mohr, C., Kurt n, T., Worsnop, D. R., and Thornton, J. A.: An Iodide-Adduct
526 High-Resolution Time-of-Flight Chemical-Ionization Mass Spectrometer: Application to Atmospheric
527 Inorganic and Organic Compounds, *Environ. Sci. Technol.*, 48(11), 6309-6317, doi:10.1021/es5003 62a,
528 2014.

529 Liu, W., Yang, H., Li, B., Xu, S.: Determination of Bromine and Iodine Speciation in Drinking Water Using High
530 Performance Liquid Chromatography - Inductively Coupled Plasma - Mass Spectrometry, *Geostand. Geoanal.*
531 *Res.*, 35, 69-74., doi:10.1111/j.1751-908X.2010.00033.x, 2015.

532 Mahajan, A.S., Sorribas, M., G omez Mart n, J.C., MacDonald, S.M., Gil, M., Plane, J.M.C., Saiz-Lopez, A.:
533 Concurrent observations of atomic iodine, molecular iodine and ultrafine particles in a coastal environment,

534 Atmos. Chem. Phys.,11, 2545-2555, doi: 10.5194/acp-11-2545-2011, 2011.

535 Mart í, J.C., G ómez, G ávez, O., Baeza-Romero, M.T., Ingham, T., Plane, J.M.C., Blitz, M.A.: On the mechanism
536 of iodine oxide particle formation, Phys. Chem. Chem. Phys., 15, 15612-15622, doi:10.1039/c3cp51217g,
537 2013.

538 McFiggans, G., Bale, C. S. E., Ball, S. M., Beames, J. M., Bloss, W. J., Carpenter, L. J., Gallagher, M. W.:
539 Iodine-mediated coastal particle formation: an overview of the Reactive Halogens in the Marine Boundary
540 Layer (RHAMBLE) Roscoff coastal study, Atmos. Chem. Phys., 10,2975-2999, doi:
541 10.5194/acp-10-2975-2010, 2010.

542 Mcfiggans, G., Coe, H., Burgess, R., Allan, J., Cubison, M., Alfarra, M. R.: Physics Direct evidence for coastal
543 iodine particles from Laminaria macroalgae – linkage to emissions of molecular iodine, Atmos. Chem. Phys.,
544 4, 701-713, doi: 10.5194/acp-4-701-2004, 2004.

545 Nayar S. and Bott K.: Current status of global cultivated seaweed production and markets, World Aquaculture
546 45(2):32-37, 2014

547 O'Dowd, C. D., Kaarle, H., Jyrki, M., Minna, V., Pasi, A., Gerrit, D. L.: Coastal new particle formation:
548 Environmental conditions and aerosol physicochemical characteristics during nucleation bursts, J. Geophys.
549 Res-atmos., 107, PAR 12-11–PAR 12-17, doi:10.1029/2000JD000206, 2002.

550 O'Dowd,C.D., Jimenez, J.L., Bahreini, R.: Marine aerosol formation from biogenic iodine emissions, Nature,
551 417(6889):632-636, doi: 10.1038/nature00775, 2002.

552 O'Dowd, C. D., De Leeuw, G.: Marine aerosol production: a review of the current knowledge, Philos. T R Soc. A.,
553 365, 1753-1774, doi:10.1098/rsta.2007.2043, 2007.

554 Palmer, C.J., Anders, T.L., Carpenter, L.J., K üpper, F.C., Mcfiggans, G.B.: Iodine and halocarbon response of
555 laminaria digitata to oxidative stress and links to atmospheric new particle production, Environ. Chem., 2,

556 282-290, doi:10.1071/EN05078, 2005.

557 Pechtl, S., Schmitz, G., von Glasow, R.: Modelling iodide-iodate speciation in atmospheric aerosol: Contributions
558 of inorganic and organic iodine chemistry, *Atmos. Chem. Phys.*, 7, 1381-1393, doi:10.5194/acp-7-1381-2007,
559 2007.

560 Redeker, K.R., Wang, N., Low, J.C., Mcmillan, A., Tyler, S.C., Cicerone, R.J.: Emissions of methyl halides and
561 methane from rice paddies, *Science*, 290, 966-969, doi:10.1126/science.290.5493.966, 2000.

562 Roscoe, H. K., Jones, A. E., Brough, N., Weller, R., Saiz-Lopez, A., Mahajan, A. S., Schoenhardt, A., Burrows, J. P.,
563 and Fleming, Z. L.: Particles and iodine compounds in coastal Antarctica, *J. Geophys. Res.-Atmos.*, 120,
564 7144-7156, doi:10.1002/2015JD023301, 2015.

565 Saiz-Lopez, A., Plane, J.M., Baker, A.R., Carpenter, L.J., Von, G.R., Mart ín, J.C., Mcfiggans, G., Saunders, R.W.:
566 Atmospheric chemistry of iodine, *Chem. Rev.*, 112, 1773-1804, doi:10.1021/cr200 029u, 2012a.

567 Saunders, R. W., Kumar, R., Gomez Martin, J. C., Mahajan, A. S., Murray, B. J., and Plane, J. M. C.: Studies of the
568 Formation and Growth of Aerosol from Molecular Iodine Precursor, *Zeitschrift Fur Physikalische*
569 *Chemie-International Journal of Research in Physical Chemistry & Chemical Physics*, 224, 1095-1117,
570 10.1524/zpch.2010.6143, 2010.

571 Sellegri, K., Yoon, Y.J., Jennings, S.G., O'Dowd, C. D., Pirjola, L., Cautenet, S.: Quantification of coastal new
572 ultra-fine particles formation from in situ and chamber measurements during the BIOFLUX campaign,
573 *Environ. Chem.*, 2, 260-270, doi:10.1071/EN05074, 2006.

574 Seto, F.Y.B., Duce, R.A.: A laboratory study of iodine enrichment on atmospheric sea-salt particles produced by
575 bubbles, *J Geophy. Res.*, 77, 5339-5349 , doi:10.1029/JC077i027p05339, 1972.

576 Shah, M., Wuilloud, R.G., Kannamkumarath, S.S., Caruso, J.A.: Iodine speciation studies in commercially
577 available seaweed by coupling different chromatographic techniques with UV and ICP-MS detection, *J Anal.*

578 Atom. Spectrom., 20, 176-182, doi:10.1039/b415756g, 2005.

579 Sipilä M., Sarnela, N., Jokinen, T., Henschel, H., Junninen, H., Kontkanen, J., Richters, S., Kangasluoma, J.,
580 Franchin, A., Peräkylä O.: Molecular-scale evidence of aerosol particle formation via sequential addition of
581 HIO₃, Nature, 537, 532, doi:10.1038/nature19314, 2016.

582 Sive, B.C., Varner, R.K., Mao, H., Blake, D.R., Wingenter, O.W., Talbot, R.: A large terrestrial source of methyl
583 iodide, Geophys. Res. Lett., 34, 251-270, doi:10.1029/2007gl030528, 2007.

584 Wang, K.E., Jiang, S.J.: Determination of iodine and bromine compounds by ion chromatography /dynamic
585 reaction cell inductively coupled plasma mass spectrometry, Anal. Sci., 24, 509-514, ,
586 doi:10.2116/analsci.24.509, 2008.

587 Wei, L., Hongxia, Y., Bing, L., Dengyun, C., Huijuan, Z.: Speciation Stabilities of Iodine in underground Water by
588 High Performance Liquid Chromatography-Inductively Coupled Plasma Mass Spectrometry, Chinese J of
589 Anal. Chem., 35, 571-573, doi: 10.1016/s1872-2040(07)60047-4, 2007.

590 Wimschneider, A., Heumann, K.G.: Iodine speciation in size fractionated atmospheric particles by isotope dilution
591 mass spectrometry, Fresen. J Anal. Chem., 353, 191-196, doi:10.1007/BF00322957, 1995.

592 Xu, S., Xie, Z., Li, B., Liu, W., Sun, L., Kang, H., Yang, H., Zhang, P.: Iodine speciation in marine aerosols along a
593 15 000-km round-trip cruise path from Shanghai, China, to the Arctic Ocean, Environ. Chem., 7, 406-412, doi:
594 10.1071/EN10048, 2010.

595 Yang, Y., Peng, Y., Chang, Q., Dan, C., Guo, W., Wang, Y.: Selective Identification of Organic Iodine Compounds
596 Using Liquid Chromatography-High Resolution Mass Spectrometry, Anal. Chem., 88, 1275, doi:
597 10.1021/acs.analchem.5b03694, 2016.

598 Yoon, Y. J., O'Dowd, C. D., Jennings, S. G., Lee, S. H.: Statistical characteristics and predictability of particle
599 formation events at Mace Head, J Geophys. Res. 111, doi:10.1029/2005JD006284, 2006.

600 Yoshida, S., Muramatsu, Y., Katou, S., Sekimoto, H.: Determination of the chemical forms of iodine with
601 IC-ICP-MS and its application to environmental samples, *J Radioanal. Nucl. Chem.*, 273, 211-214,
602 doi:10.1007/s10967-007-0738-4, 2007.

603 Yu, H. , Zhou, L., Dai, L., Shen, W., Dai, W., Zheng, J.: Nucleation and growth of sub-3 nm particles in the polluted
604 urban atmosphere of a megacity in China, *Atmos. Chem. Phys.*, 16, 18653-18690,
605 doi:10.5194/acp-16-2641-2016, 2016.

606 Yu, H., Wu, C., Wu, D., Yu, J. Z.: Size Distributions of Elemental Carbon and its Contribution to Light Extinction
607 in Urban and Rural Locations in the Pearl River Delta region, China, *Atmos. Chem. Phys.*, 10: 5107-5119,
608 doi:10.5194/acp-10-5107-2010, 2010.

609 Yun, L., Peng, Y., Chang, Q., Zhu, Q., Guo, W., Wang, Y.: Identification of Organic Iodine Compounds and their
610 Transformation Products in Edible Iodized Salt using Liquid Chromatography-High Resolution Mass
611 Spectrometry, *J Agr. Food Chem.*, 65, 5384-5389, doi:10.1021/acs.jafc.7b01759, 2017.

612 Zhang, X.: A picture of polar iodinated disinfection byproducts in drinking water by (UPLC/)ESI-tqMS, *Environ.*
613 *Sci. Technol.*,43, 9287., doi:10.1021/es901821a, 2009.

614 Zhang, W., Liu, X., Jia, X., Yi, H., Liu, X., Xie, X., Lu, J., Duan, T., Chen, H.: Fast Speciation of Iodide and Iodate
615 in Edible Salts and Human Urine by Short Column IC Coupled with Inductively Coupled Plasma MS,
616 *Chromatographia.*, 72, 1009-1012, doi:10.1365/s10337-010-1756-x, 2010.

Table 1. Organic iodine compounds that were detected at least once in the aerosol samples. n: the number of samples. Four PM_{2.5} samples were collected at the inland site; three PM_{2.5} samples and three sets of nano-MOUDI samples were collected at the coastal site. m/n numbers in right 4 columns: a given molecular formula was detected in m out of n samples. A blank cell means the formula was not detected in any samples. Also shown are measured ion mass, exact ion mass and the number of isomers based on the number of chromatographic peaks observed for given ion mass in the samples. Bold formulas are observed in ESI+ mode and others in ESI- mode.

Molecular formula	Measured ion mass (Da)	exact ion mass (Da)	Isomer number	Coastal site (n=6)			Inland site (n=4)	All samples
				I-NPF	Continent al NPF	Non-NPF		
C ₂ H ₃ O ₂ I	184.9099	184.9099	1	3/4	1/1	1/1	4/4	9/10
C ₃ H ₃ O ₂ I	196.9098	196.9099	1	4/4	1/1		1/4	6/10
CH ₂ I ₂	266.8177	266.8168	1	3/4	1/1		1/4	5/10
C ₂ H ₂ O ₂ I ₂	310.8079	310.8066	1	4/4				4/10
CH ₂ SO ₃ I ₂	346.7743	346.7736	1	2/4	1/1			3/10
C ₆ H ₄ NO ₄ I	279.9112	279.9107	1	3/4	1/1	1/1	4/4	9/10
C ₁₀ H ₆ NO ₃ I	313.9319	313.9314	1	4/4	1/1	1/1	3/4	9/10
C ₆ H ₄ NO ₃ I	263.9164	263.9158	1	4/4	1/1	1/1	2/4	8/10
C ₇ H ₆ NO ₄ I	293.9269	293.9263	2	3/4	1/1			4/10
C₅H₄NOI	221.9414	221.9416	2	3/4				3/10
C₆H₆NOI	235.9571	235.9572	2	3/4				3/10
C₇H₈NOI	249.9726	249.9729	3	3/4				3/10
C ₉ H ₁₀ NO ₄ I	321.9572	321.9576	2	1/4	1/1		1/4	3/10
C ₈ H ₆ NO ₅ I	321.9216	321.9212	1	2/4				2/10
C₉H₆NOI	271.9570	271.9572	2	2/4				2/10
C ₈ H ₈ NO ₅ I	323.9370	323.9369	1	1/4				1/10
C ₈ H ₇ O ₂ I	260.9411	260.9412	1	3/4	1/1	1/1	2/4	7/10
C ₇ H ₅ O ₄ I	278.9156	278.9154	2	2/4	1/1	1/1	2/4	6/10
C ₇ H ₅ O ₂ I	246.9260	246.9256	1	3/4	1/1		1/4	5/10
C ₈ H ₅ O ₃ I	274.9210	274.9205	1		1/1		2/4	3/10
C ₆ H ₃ OI ₃	470.7245	470.7240	1	1/4	1/1			2/10
C ₇ H ₄ O ₃ I ₂	388.8177	388.8172	1	1/4	1/1			2/10
C ₇ H ₅ O ₃ I	262.9209	262.9205	2	1/4	1/1			2/10
C ₇ H ₆ O ₂ I ₂	374.8383	374.8379	1	1/4	1/1			2/10
C ₇ H ₇ O ₄ I	280.9298	280.9311	1	2/4				2/10
C ₈ H ₄ O ₂ I ₂	372.8230	372.8222	1	1/4	1/1			2/10
C ₈ H ₆ O ₂ I ₂	386.8382	386.8379	1	1/4	1/1			2/10
C ₈ H ₆ O ₃ I ₂	402.8319	402.8328	1	1/4	1/1			2/10
C ₈ H ₇ O ₃ I	276.9361	276.9362	1	1/4	1/1			2/10
C ₈ H ₈ O ₃ I ₂	404.8489	404.8485	1	2/4				2/10
C ₉ H ₇ O ₃ I	288.9372	288.9362	1	1/4				1/10
C ₉ H ₇ O ₄ I	304.9309	304.9311	2	1/4				1/10
C₇H₁₁N₂I	251.0044	251.0045	1	3/4			1/4	4/10
C₈H₁₁N₆I	319.0172	319.0168	1	1/4				1/10

C₄H₄N₂I₂ 334.8547 334.8542 1 1/1 1/10

Table 2. Comparison of iodine species in PM_{2.5} between the inland urban site and the coastal site. iodide: the sum of I⁻, I₃⁻ and I⁻-metal complexes (if present). IO_x⁻: the sum of IO₃⁻, IO₂⁻ and IO⁻; SOI: soluble organic iodine that is calculated as the difference between total iodine and the sum of iodide and IO_x⁻. I-AA: the sum of iodoacetic acid and diiodoacetic acid; I-PA: iodopropenoic acid; I-MSA: iodomethanesulfonic acid; CHI₂⁻: diiodomethane; I-aromatics: total aromatic iodine compounds; I-organic adducts: iodide-organic adducts. Also shown are iodine species measured by IC-ICP-MS at Mace Head (Gilfedder et al., 2008), an Ireland coastal site, and Regensburg (Wimschneider and Heumann, 1995), an inland site of southern Germany. %: the percentages of iodine species in total iodine.

Iodine species	Inland site (n=4)		Coastal site (n=6)		Mace Head, Ireland		Regensburg, Germany	
	Conc. (pmol m ⁻³)	%	Conc. (pmol m ⁻³)	%	Conc. (pmol m ⁻³)	%	Conc (pmol m ⁻³)	%
iodide	1.0-3.7	23 ± 9	3.8-74.1	31 ± 14	0.3-58	3.7-30	3.1-7.2	12-31
IO _x ⁻	ND-0.087	0.3 ± 0.6	1.5-53.1	23 ± 14	nd-15	0.1-7.2	12.6-54.2	69-88
SOI	5.4-7.5	77 ± 9	14.2-66.1	46 ± 27	3.7-509	69-96		
I-organic adducts	4.3-6.1	64 ± 8	6.7-62.9	31 ± 16				
CHI ₂ I ⁻	ND-0.083	0.2 ± 0.4	0.036-0.74	0.4 ± 0.7				
I-AA	0.054-0.25	1.6 ± 1.0	0.57-2.2	4.8 ± 5.6				
I-MSA	ND	0	ND-0.28	0.09 ± 0.12				
I-PA	ND-0.016	0.04 ± 0.07	0.16-5.2	5.9 ± 4.6				
I-aromatics	0.76-1.2	12 ± 3	0.1-12.3	6.7 ± 6.8				
Total Iodine	6.5-11.2		19.5-122.6		10-532		15.7-61.3	

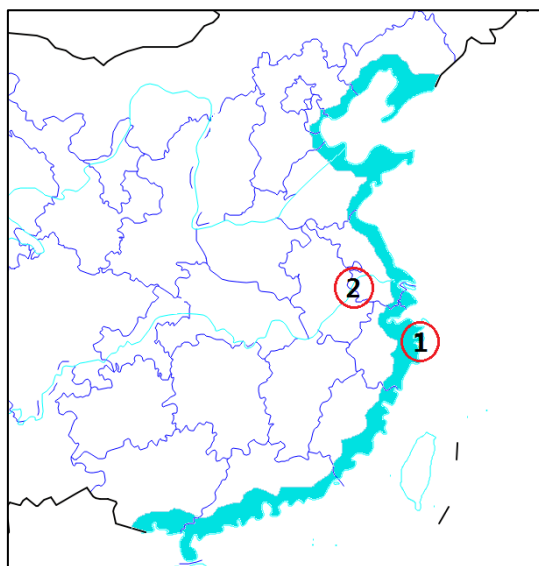


Figure 1. Locations of two sampling sites: ① the coastal site at Xiangshan Gulf ② the inland urban site that is 200 km from the coast. The blue color indicates the coastal area of China mainland.

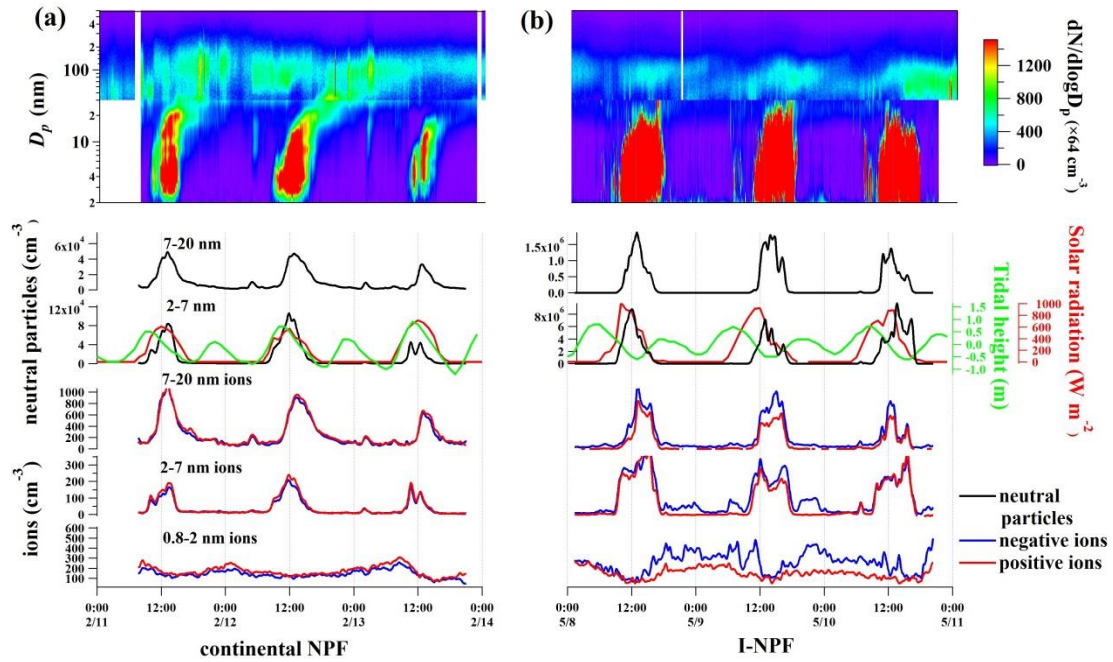


Figure 2. Particle number concentration during (a) the continental NPF days from February 11 to 13, 2018 and (b) the iodine-induced NPF (I-NPF) days from May 8 to 11, 2018. From top to bottom: particle size spectra of the NPF events; diurnal variations of 7-20 nm and 2-7 nm neutral particles (black curves); diurnal variations of 7-20 nm, 2-7 nm and 0.8-2 nm negative (blue curves) and positive ions (red curves). Solar radiation and tidal height were obtained from local maritime authority and plotted as red and green curves, respectively.

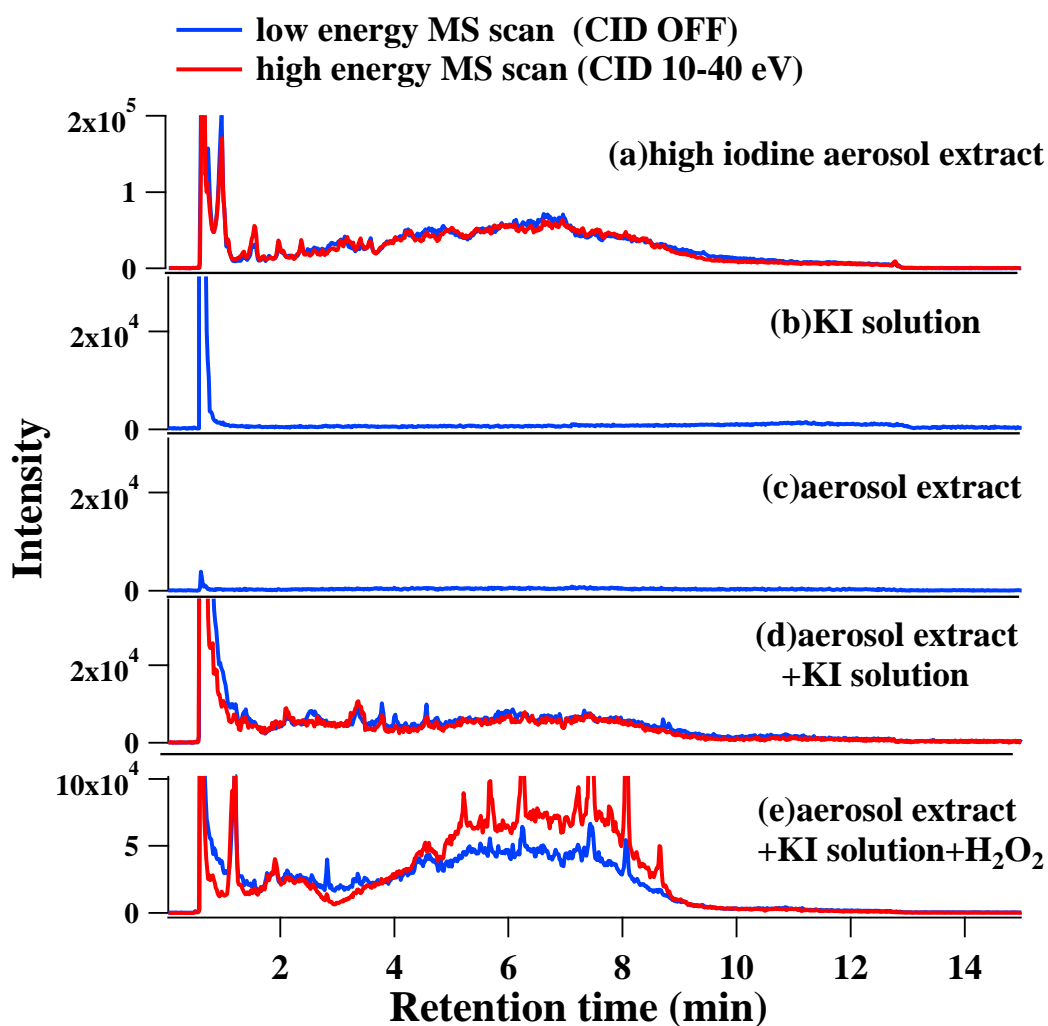


Figure 3. Ion chromatograms of m/z 126.9039 of (a) aerosol extract with high concentration of iodine, (b) pure potassium iodide (KI) solution (1 mmol L^{-1}), (c) aerosol extract with low concentration of iodine, (d) the KI solution mixed with the aerosol extract with low concentration of iodine and (e) The KI solution+aerosol extract mixture with the addition of $10 \text{ mmol L}^{-1} H_2O_2$ solution. Blue curves: low energy MS scan mode, in which collision induced dissociation is off and molecular ions are subject to in-source fragmentation only. Red curves: high energy MS scan mode, in which molecular ion are subject to both in-source fragmentation and 10-40 eV collision induced dissociation.

	Steps	MS method	Data acquired
1	MD vs. m/z diagram comparison between aerosol and aerosol+KI+H ₂ O ₂ /O ₃	Low energy MS scan	m/z and RT of potential organic iodine ions
	↓		
2	Elemental composition calculation Chemspider search	MSMS confirmation	80 possible CHONSI chemical formulas
	↓		
3	Targeted screening in real aerosol samples based on m/z and RT	Low energy MS scan	35 formulas (47 organic iodine compounds) and their peak area observed in aerosol samples
	↓		
4	4 compounds quantified with their standards; 43 compounds semi-quantified with surrogate standards	Low energy MS scan of commercial standards	Concentrations of individual non-aromatic compounds and total aromatic iodine compounds

Figure 4. Identification and semi-quantification steps of unknown organic iodine compounds in ambient aerosols

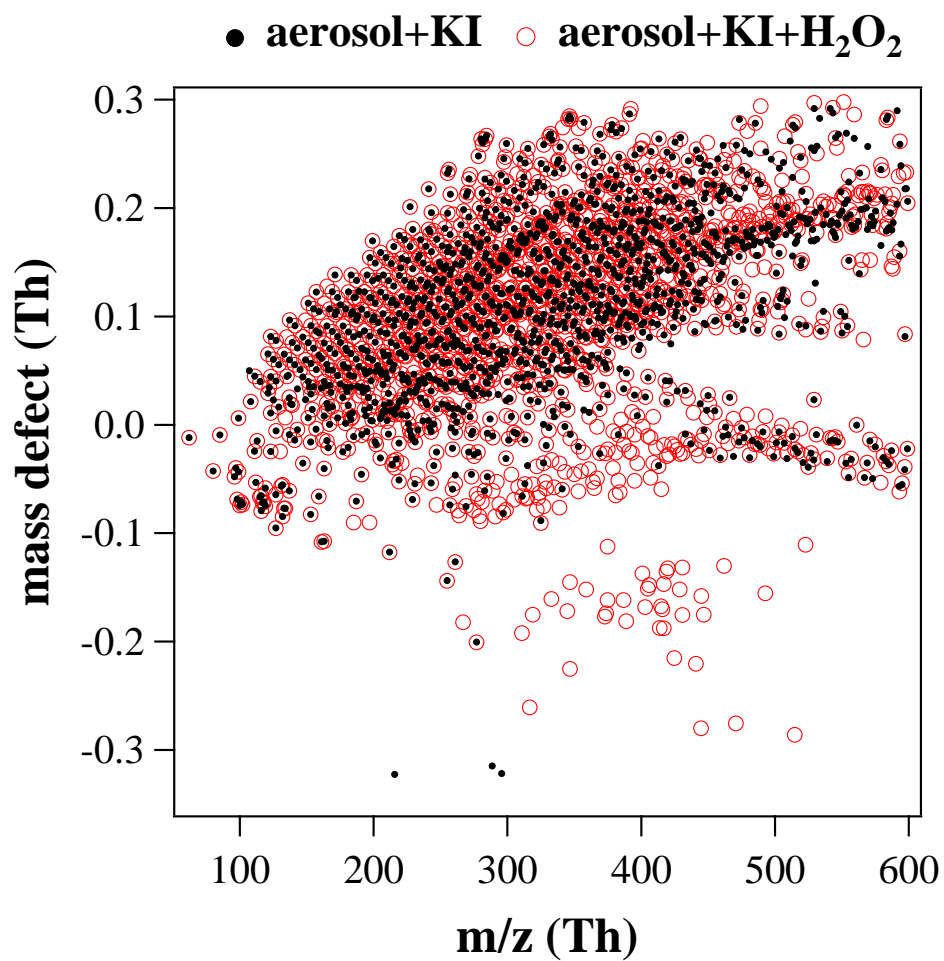


Figure 5. Mass defect (MD) vs. m/z diagram of molecular ions before (black dots) and after (red circles) the addition of H₂O₂ into aerosol extract+KI mixture. The mass spectrum of all ions above background level (10^4) was reconstructed by integrating over retention time 0-15 min.

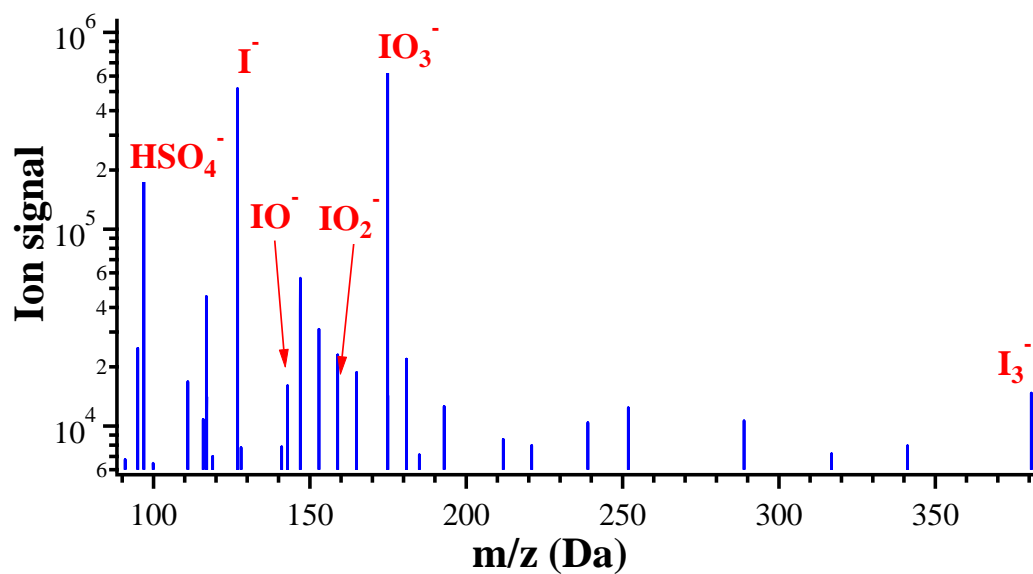


Figure 6. Integrated mass spectrum of molecular ions between retention time 0.5-0.7 min of an S13 nano-MOUDI sample (10-18 nm particles).

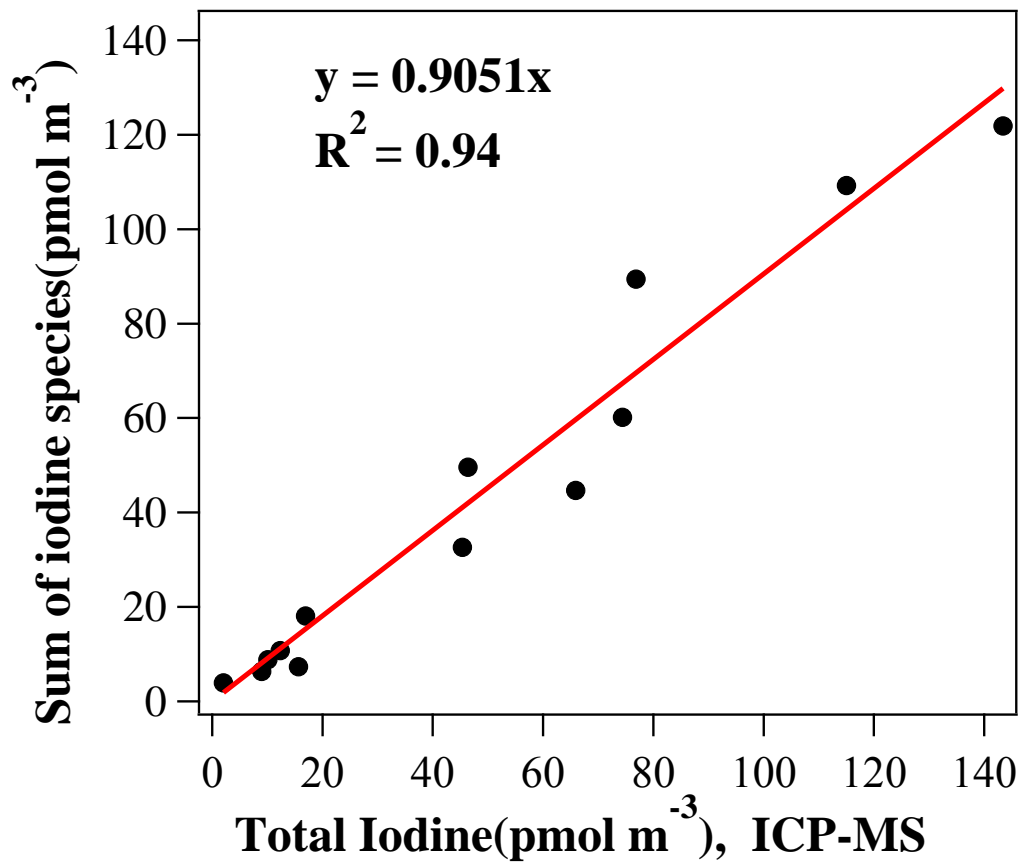


Figure 7. A comparison between the sum of all iodine species measured by our method and total iodine concentration measured by ICP-MS. Red line shows the linear regression between the two methods with a R^2 of 0.94.

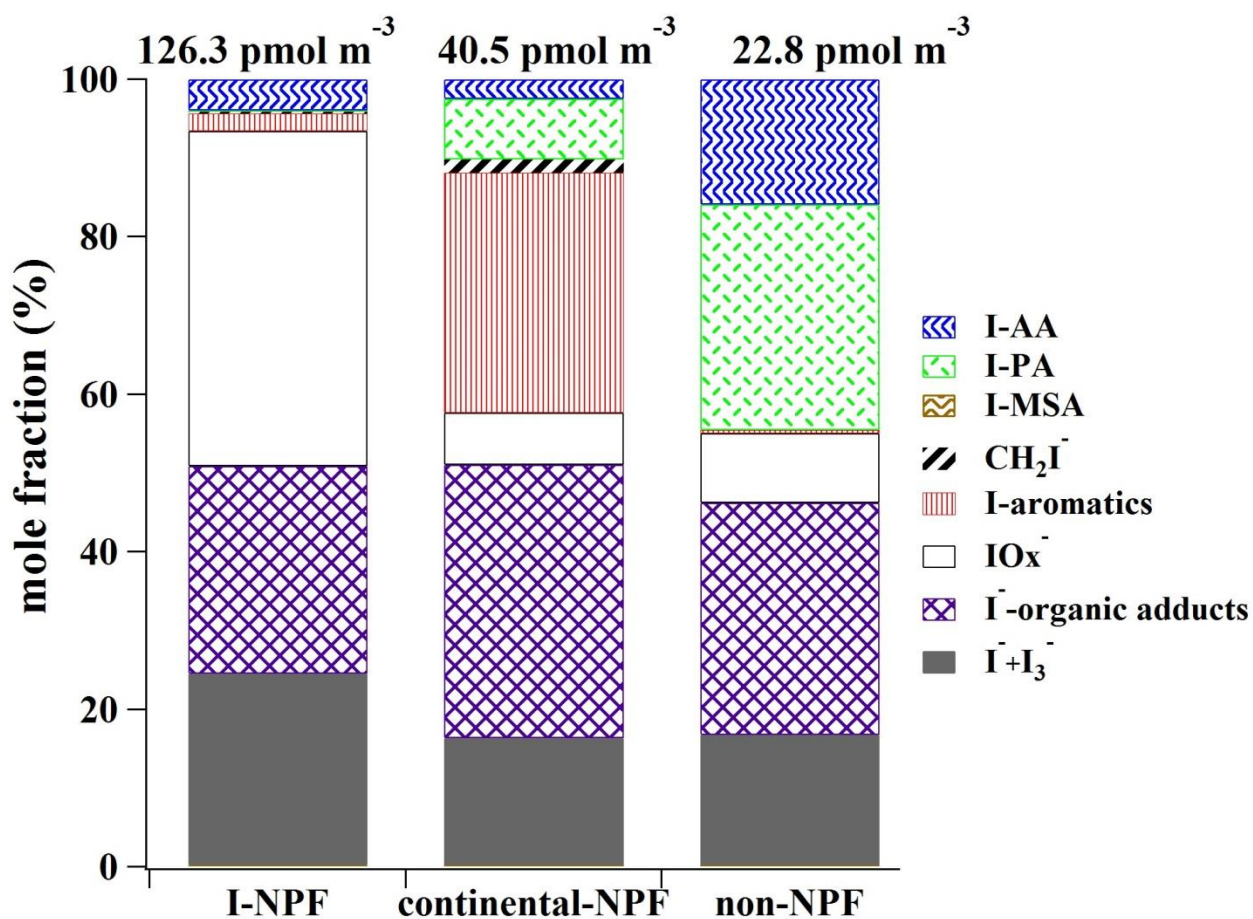


Figure 8. Total concentrations and mole fractions of iodine species in 10 nm-18 μm particles during the iodine-induced NPF (I-NPF), continental NPF and non-NPF days. I-AA: the sum of iodoacetic acid and diiodoacetic acid; I-PA: iodopropenoic acid; I-MSA: iodomethanesulfonic acid; CH_2I^- : diiodomethane; I-aromatics: total aromatic iodine compounds; IO_x^- : $[\text{IO}_3^-] + [\text{IO}_2^-] + [\text{IO}^-]$; I⁻-organic adducts: iodide-organic adducts; $\text{I}^- + \text{I}_3^-$: the sum of iodide and triiodide.

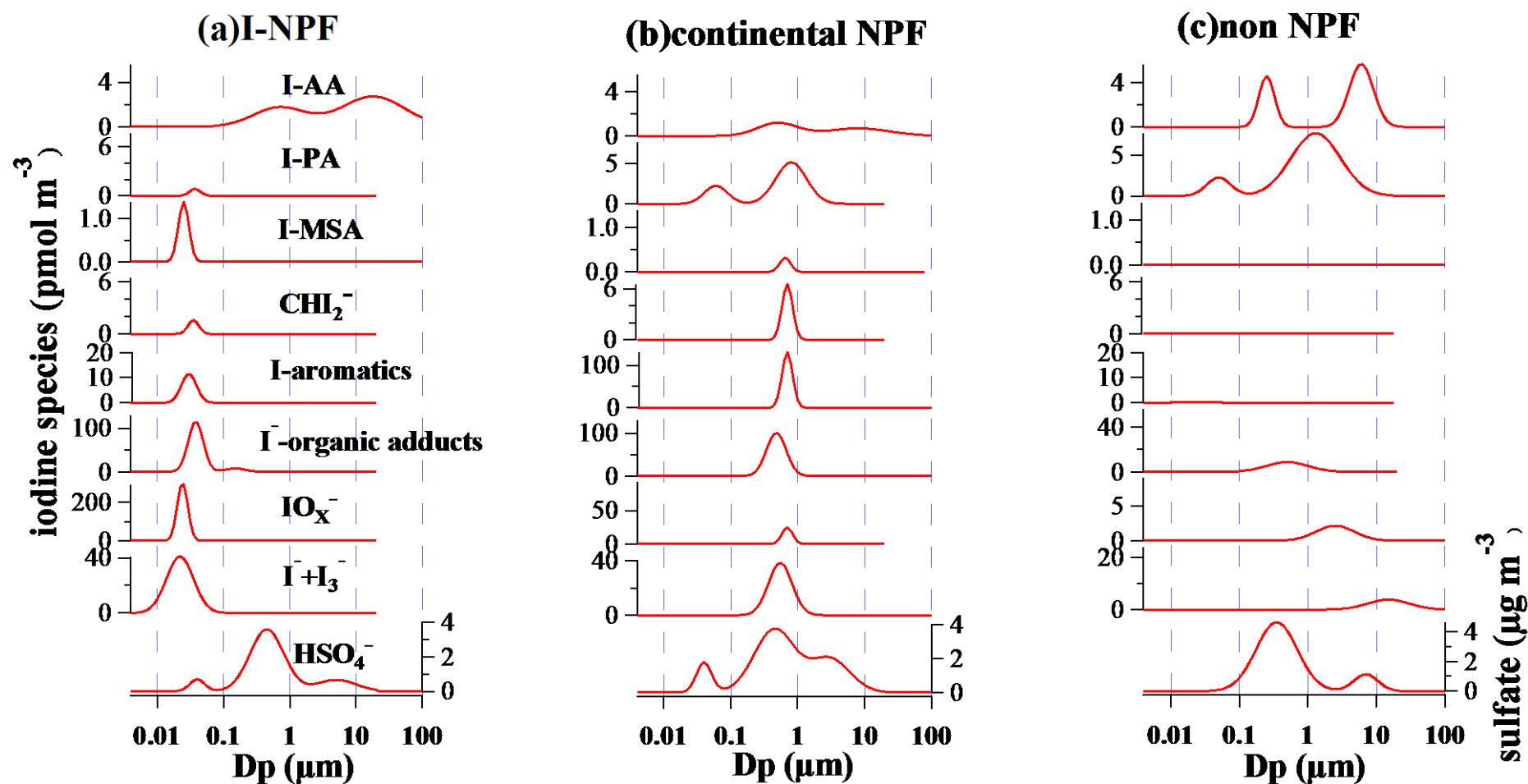


Figure 9. Mass size distribution of iodine species in 10 nm-18 μm particles during (a) iodine-induced NPF (I-NPF) days, (b) continental NPF days and (c) non-NPF days. Continuous size distributions of iodine species were inverted from the measured mass concentrations in the 13 size bins of nano-MOUDI. I-AA: the sum of iodoacetic acid and diiodoacetic acid; I-PA: iodopropenoic acid; I-MSA: iodomethanesulfonic acid; CHI_2^- : diiodomethane; I-aromatics: total aromatic iodine compounds; IO_x^- : $[\text{IO}_3^-] + [\text{IO}_2^-] + [\text{IO}^-]$; I-organic adducts: iodide-organic adducts; $\text{I}^- + \text{I}_3^-$: the sum of iodide and triiodide